

Analysis of the Blackfoot 3C-3D VSP survey

Qi Zhang, Robert R. Stewart, John M. Parkin*, and Zandong Sun

ABSTRACT

A 3C-3D vertical seismic profile (VSP) was conducted in November 1995 over the Blackfoot Field, which is located in Township 23, Range 23W4, about 15 kilometers southeast of Strathmore Alberta. The survey was acquired in the PCP 12-16-23-23W4 well. Acquisition of the survey was performed simultaneously with the Blackfoot 3C-3D surface seismic program. A total of 431 surface shots were received by a five-level tool. The simultaneous acquisition of a 3-D surface and borehole data on land is to our knowledge, one of the first of its kind. The processing techniques used here include field data preprocessing, wavefield separation, deconvolution, statics correction, NMO-correction and depth-variant mapping and stack for both P-P and P-S data. A 3-D image is produced with reasonable quality compared to other VSP and surface data. The 3C-3D VSP images tie well with the 3C-3D surface seismic and well log synthetics.

INTRODUCTION

The 3C-3D Vertical Seismic Profile (VSP) and 3C-3D surface seismic survey was conducted over the Blackfoot Field, which is owned and operated by PanCanadian Petroleum Ltd. The Blackfoot oil pool is located in Township 23, Range 23W4 about 15 kilometers southeast of Strathmore, Alberta. There has been extensive seismic work done in this area by PanCanadian and the CREWES project, including a broad-band, 3-C seismic survey in July of 1995.

In this experiment, the data were recorded downhole while a 3-D surface seismic survey was conducted. Western Atlas' MultiLevel Receiver (MLR) tool was used to record the borehole data. There are a number of ways to acquire a 3C-3D VSP. The Blackfoot 3-D VSP was cost-effective since acquisition occurred during a conventional 3-D surface seismic survey by passive and simultaneous monitoring of surface shots. We attempted to simulate longer vertical arrays by moving the five-level receiver string up and down the wellbore for various shots. The survey was originally intended to have the receiver tools located deeper in the well for near-offset shots to obtain high resolution coverage of the target near the wellbore and good velocity control. The tool would then be moved progressively shallower for farther offset shots to provide greater offset coverage. During acquisition, this regularity was not logistically practical due to the rapid shooting sequence of the surface 3D from essentially random shot locations. Over the course of the survey, the receiver tool was moved seven times (75 m each time) to give a receiver depth range from 400 m to 910 m.

The three-component data were processed by both the CREWES Project and Western Atlas. A 3-D volume rectangular and radial, depth-variant binning programs were developed for processing the data. In this paper, the results of the CREWES processing are discussed. The survey covered an area 2500 m by 2600 m. The subsurface image at target zone is about one square kilometer.

* Western Atlas international downhole seismic services.

SURVEY ACQUISITION

The 3C-3D VSP survey was designed to simultaneously record the shots from the 3C-3D surface survey. The VSP survey was acquired from 431 source locations using 4 kg dynamite charges in 18 m holes. The shot locations are shown by the light color in Figure 1. The target zone is around depth of 1600 m. The shot parameters were designed to meet the criteria of the surface seismic survey and were not optimized for the 3C-3D VSP experiment. There are 12 shot lines in the N-S direction with a line interval of 210 m. Each line includes approximately 38 shots with a shot interval of 60 m. The shot coverage in the 3-D VSP is about 2500 m East-West by 2600 m North-South. The receiver well was located on the North side of shot line 35 (see Figure 1).

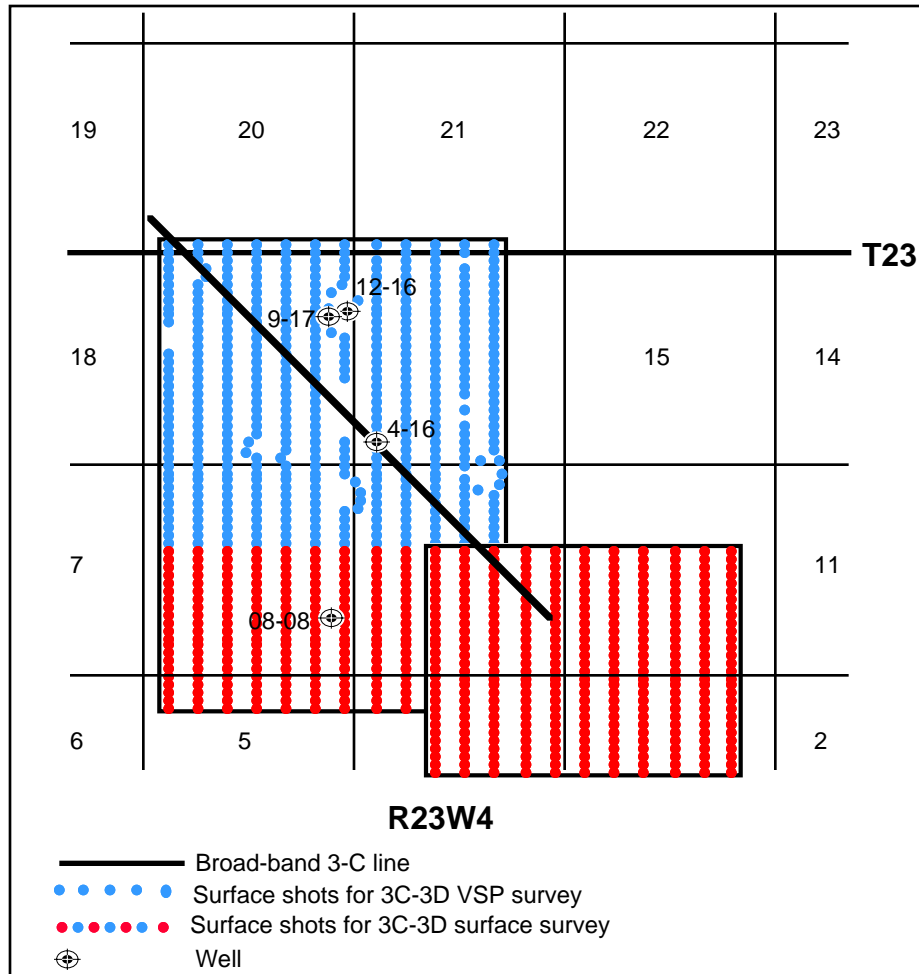


Fig. 1. Map of Blackfoot surveys showing shot points for the full 3C-3D survey, selected wells, and a previous broad-band line.

The data were recorded for 4 seconds at a 1 ms sample rate using the Western Atlas five-level, three-component MultiLevel Receiver (MLR) tool. The MLR consists of five 1.2 m long tools separated by 15 m wireline interconnects. Inside each tool are three orthogonal and gimbal-mounted 10 Hz geophones. Each tool is individually coupled to the borehole by a surface-controlled mechanical arm supplying an 8:1 coupling force in open or cased wellbores. The data are digitized downhole at the top of the tool string and transmitted to the surface.

Shooting of the surface grid was performed by up to 4 shooters operating on the grid from a variety of offset locations. While this method results in efficient surface acquisition, it did not allow for optimal source and downhole receiver geometry to create an even subsurface coverage. We decided that the MLR would acquire about 40 shots before moving to the next interval. The data were recorded at 35 levels between the depths of 910 m to 400 m at a 15 m interval. Most shots are recorded with receivers located in the range of 400 m to 685 m in order to obtain more data from a wider offset coverage. Figure 2 shows surface shot and the associated the receiver depth.

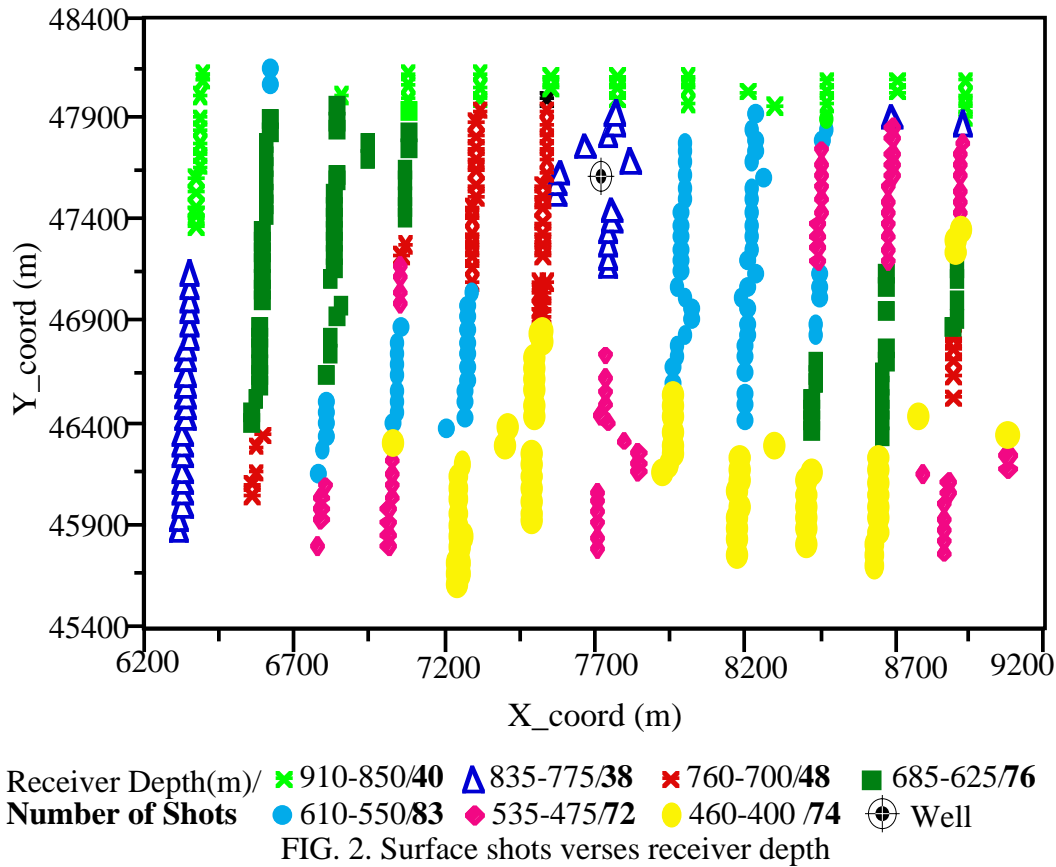


FIG. 2. Surface shots verses receiver depth

This addition of the 3C-3D VSP to the Blackfoot study was initiated only several days before acquisition was to begin. Since the Western Atlas acquisition system is normally a standalone recorder, a number of technical hardware and software challenges had to be overcome. Working with the surface acquisition company, Veritas DGC and Western Atlas, the recorder was successfully slaved to the Veritas recorder via radio and a recording method was devised. As a timing verification, a geophone spread near the wellhead was patched into the Western Atlas recorder. When the Veritas Observer gave the 'alert', the Western Atlas engineer armed the VSP recording software. The recorder was then triggered remotely by the Veritas recorder and built in delays insured the time break confirmation was recorded for 97 % of the shots. The vertical data channel, time break and surface spread were verified in real time on the Western Atlas computer screen. The system was then reset for the next shot. This cycle required approximately 15 seconds that allowed the surface acquisition to proceed without impedance from the borehole acquisition. After a given series of shots were recorded the receiver locking arms were retracted and the MLR was move to the next interval. Maximum of 5 minutes was required to unclamp, move and reclamp the tools to the wellbore.

The data were acquired in a cased wellbore. No information about the quality of the cement behind casing was available. Data quality is often dependent on how well the casing is cemented to the wellbore. Where no cement exists, one can reasonably expect a certain amount of sloughing behind the casing to fill the void and provide some coupling. Nevertheless, casing ring was evident on many shots.

DATA PROCESSING

Pre-processing

The data were preprocessed by Western Atlas. Using the time break channel recorded with each shot, the data were shifted to their true ‘time zero’ position. The first arrivals were then picked on the vertical component and applied to the horizontal components. Hodogram analysis was performed on the data to maximize the energy into a single component in the source receiver plane, termed the radial component. Figure 3a shows the hodogram analysis for a single receiver and the horizontal data before and after rotation. The horizontal channel 1 (H1) and channel 2 (H2) data are analyzed in a small window encompassing the direct arrival to determine the tool orientation at each level. Hodograms are computed based on the particle motion between the two horizontal traces. At each depth level, the major axis of the ellipse defined by the hodogram was used to determine the rotation angle needed to align the one horizontal component in the direction of the source. After rotation, the maximized horizontal component pointing in the direction of the source is termed the Radial component and the minimized horizontal data is called the Transverse component. Figure 3b shows a single shot of receiver traces after rotation. Relative amplitude between the components is maintained so that the Radial and Transverse components may be compared. Note the casing ring on the deepest receiver indicates poor coupling of the casing and the formation.

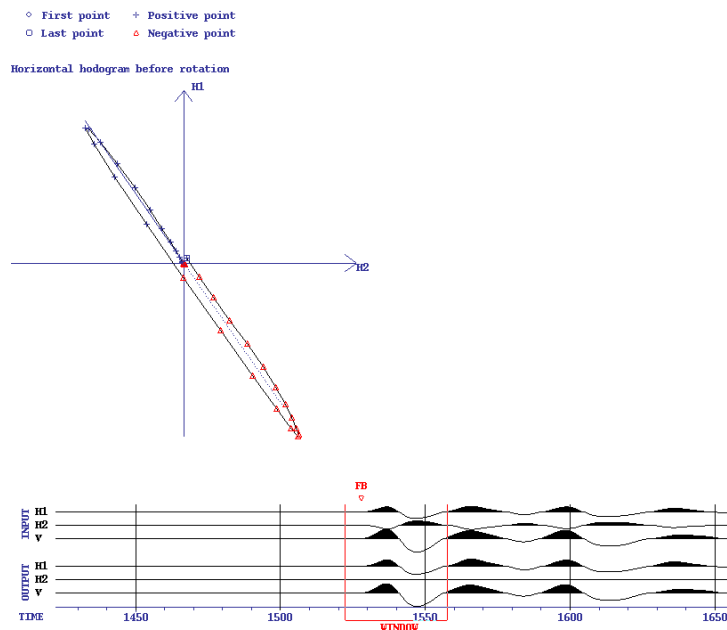


FIG. 3(a). Hodogram plot of horizontal components. Three-component data before and after rotation

Using the time break channel recorded with each shot, the data were shifted to their true 'time zero' position. The first arrivals were then picked on the vertical component and applied to the horizontal components. Hodogram analysis was performed on the data to maximize the energy into a single component in the source receiver plane, termed the radial component. Figure 3a shows the hodogram analysis for a single receiver and the horizontal data before and after rotation. The horizontal channel 1 (H1) and channel 2 (H2) data are analyzed in a small window encompassing the direct arrival to determine the tool orientation at each level. Hodograms are computed based on the particle motion between the two horizontal traces. At each depth level, the major axis of the ellipse defined by the hodogram was used to determine the rotation angle needed to align the one horizontal component in the direction of the source. After rotation, the maximized horizontal component pointing in the direction of the source is termed the Radial component and the minimized horizontal data is called the Transverse component. Figure 3b shows a single shot of receiver traces after rotation. Relative amplitude between the components is maintained so that the Radial and Transverse components may be compared. Note the casing ring on the deepest receiver indicating poor coupling of the casing and the formation.

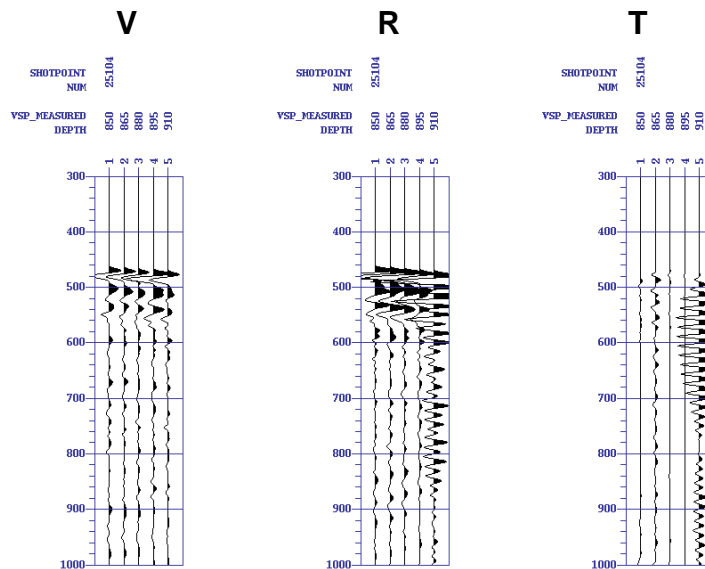


FIG. 3b. 3-C data after rotation from one shot and single tool position.

Raw data analysis

Each component dataset consists of 431, 5 trace shot gathers. The data shown in Figure 4 are four 3-component shot gathers. The vertical axis is in time and the horizontal axis is the receiver depth. VSP data are recorded in the time- depth domain instead of the time-offset domain of surface seismic. In any given shot gather, the downgoing wave has a moveout increasing in time from the shallow receiver on the left to the deep receiver on the right. The reflected wave has a moveout decreasing in time from deep to shallow. The first arrival times depend on the source offset and the receiver depth. It is only in the shot gather that the different wavefields can be easily separated since transmitted and reflected wavefields have opposite moveouts. Figure 5 to 6 shows the shot-sorted vertical and radial component data recorded from shot line 31. The corresponding receiver depths for these shots are from 400 to 910 m. First arrival times and wavefield moveouts are as in Figure 4, so the reflection events can not

be viewed continuously from shot to shot without mapping to a normal incidence, two-way travel-time. Figure 7 and 8 are common receiver gathers for the vertical and radial components at depths of 400, 475, 565, 880 m. In each receiver gather, the data are sorted by absolute offset. In this figure, we see coherent events, but the downgoing and upgoing wave modes will have similar instead of opposite moveouts as in the shot gather. The large change on the first arrivals at depth of 475 m is due to the abrupt change of offsets recorded at this depth.

The reflected upgoing and transmitted downgoing wave modes can best be differentiated in the shot gather, allowing for the wavefields to be separated in this domain. Before separation the data in a receiver gather show the time delay due to the source-receiver offset but is of little use in identifying reflections. The shot statics-corrections can be done in receiver gather before wavefield separation, and residual statics can be corrected in this gather alternatively with NMO-correction. The CDP gather can not be obtained during the geometry assignment since because the reflections on a given trace are offset as well as depth variant. Creating CDP gathers is done in the reflection mapping and imaging stage.

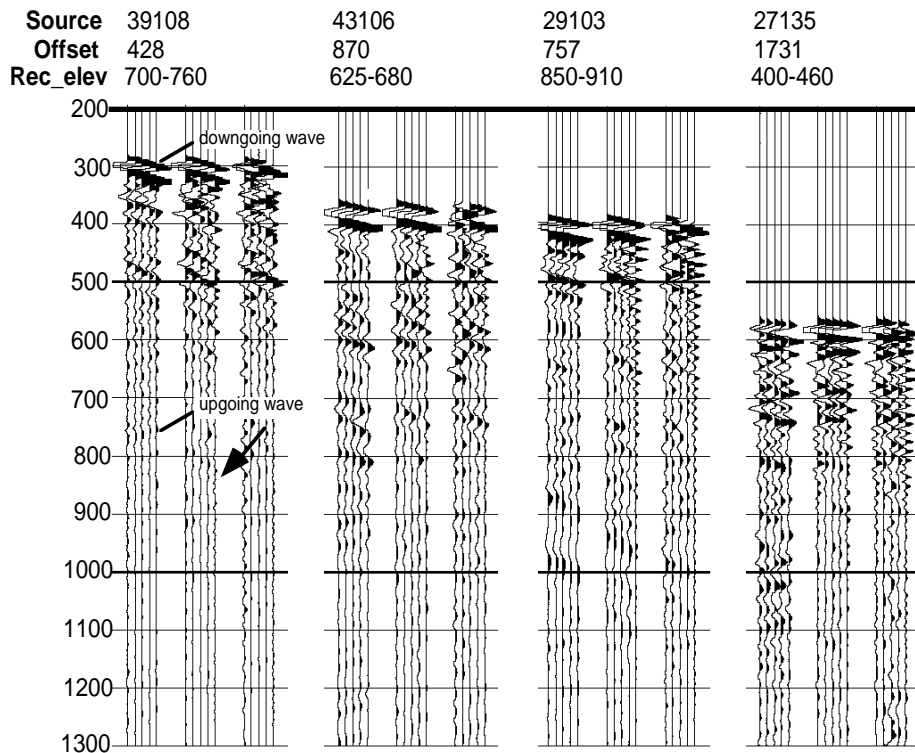


FIG. 4. Raw shot gathers from 4 sources. Each set of traces contains 5 - vertical, 5 - H1, and 5 - H2 components displayed from left to right. Data have been trace normalized.

Statics correction and amplitude recovery

Shot statics computed from the surface 3-D data was applied to the vertical and radial components. Since the receivers are in the wellbore and the reflected wave does not travel through weathering layer, only shot statics corrections are required. Amplitude compensation for loss due to spherical divergence on the vertical component was made.

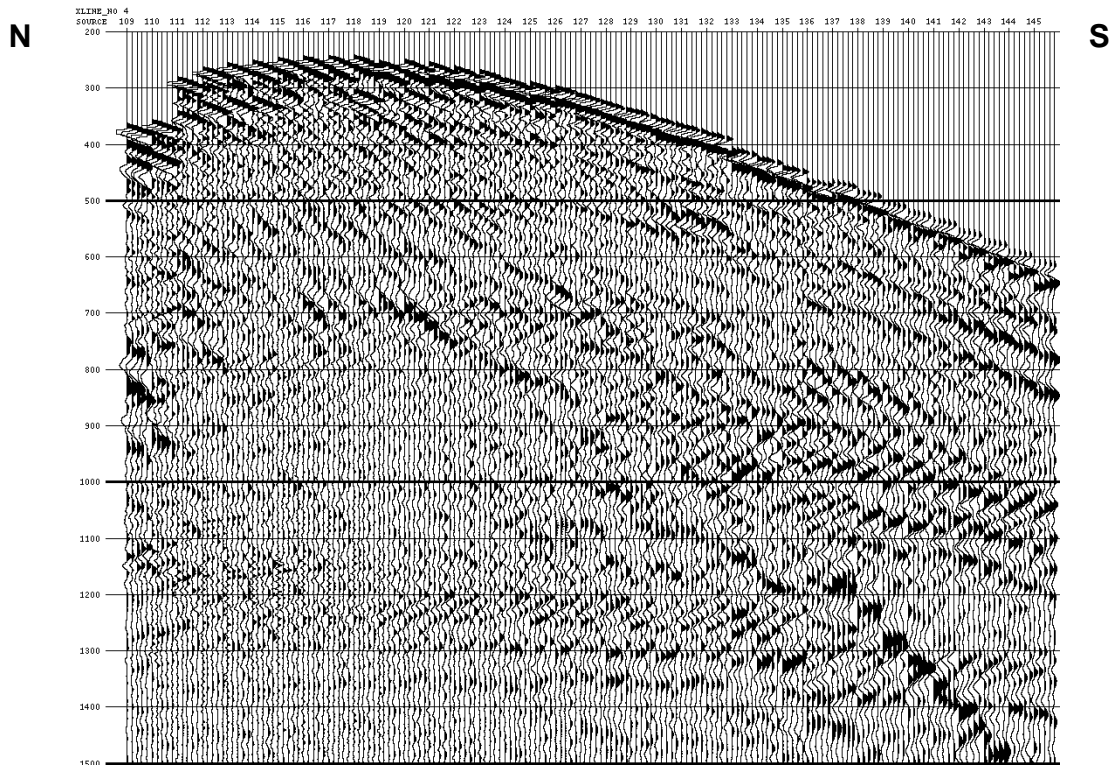


FIG. 5. trace equalized vertical component raw data of shot line 31. Traces from each shot are sorted in increasing.

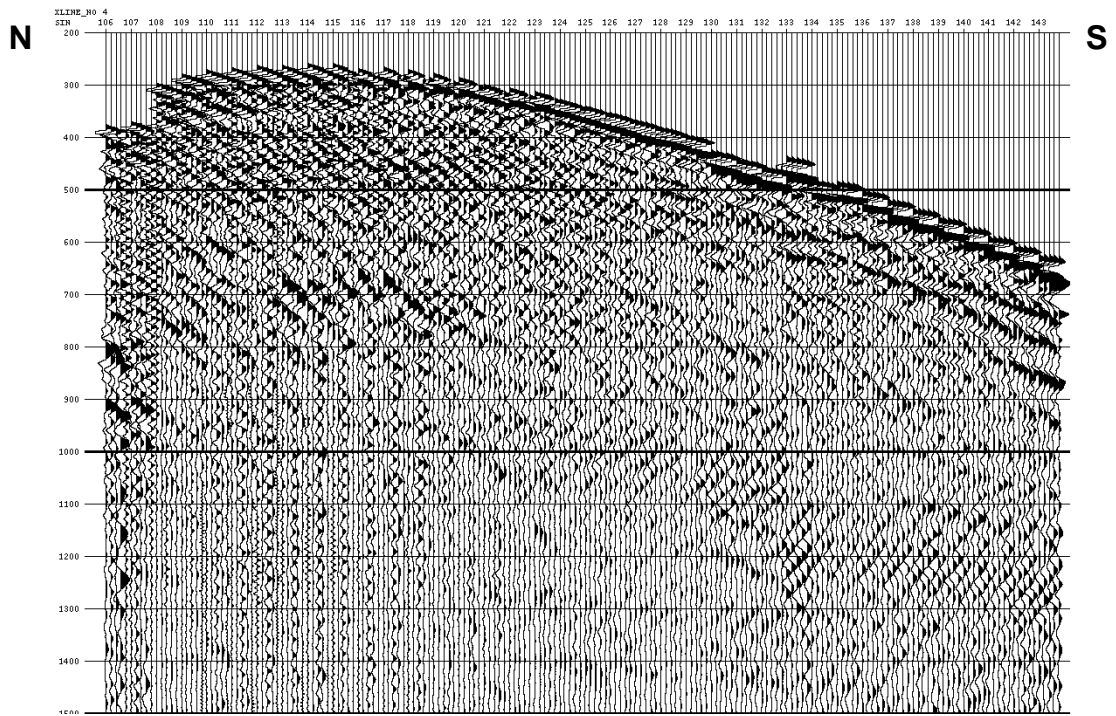


FIG. 6. Trace equalized radial-component raw data of shot line 31. Traces from each shot are sorted in increasing receiver depth.

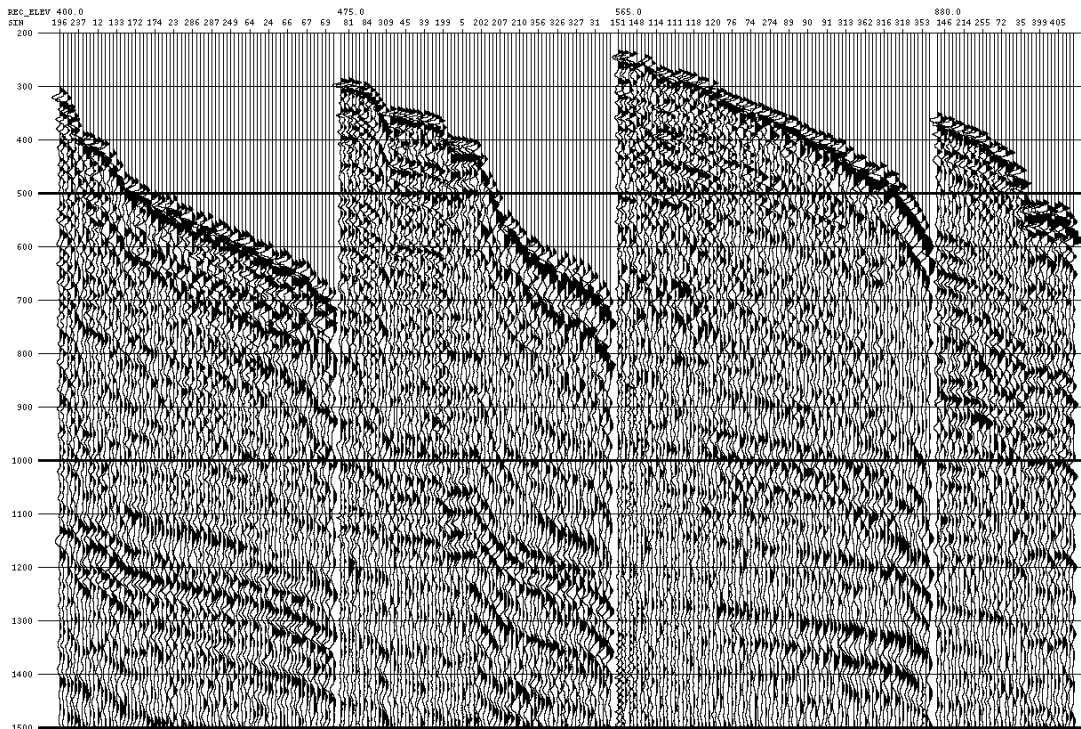
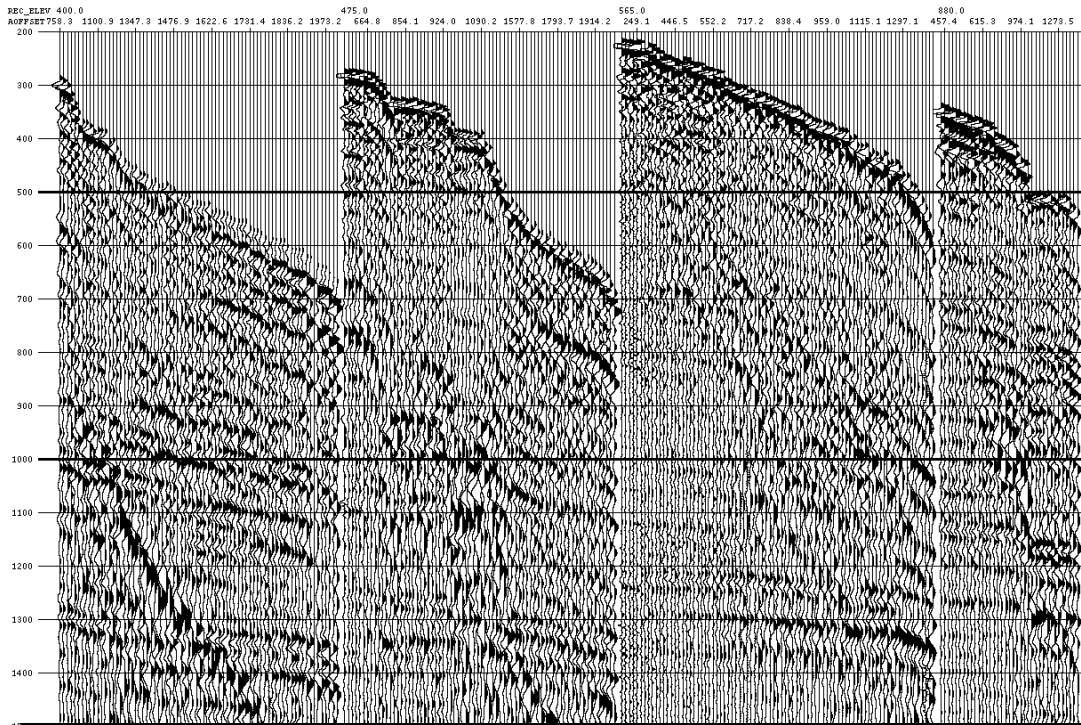


Fig. 7 (top) and Fig 8 (bottom): Trace equalized common receiver gathers. Top: vertical component data. Bottom: Radial component data. Traces in each gather are sorted in increasing offset order.

using the velocity information from the 2-D seismic (Gorek et al. 1995). A trace balance using a window of 2500 ms follows amplitude recovery. The gain and trace

balance parameters computed from the vertical component were then applied to the radial component dataset.

Signal analysis

Frequency analysis of the raw vertical component was performed using the f-x prediction filter method developed by Margrave (1995). The purpose of this signal analysis is to evaluate the amplitude and phase signature to determine the average parameters of full dataset. The data in the analysis has been pre-processed and flattened on its first arrival.

Figure 9 shows the vertical data from shot-line 39. It is flattened on the first arrival and sorted by shot in the North - South direction. The signal analysis is done on the high-lighted zones in Figure 9. Zones 1 and 2 are the first arrivals for at the North and South ends of line 39. Zone 3 is the upgoing wave on the North end of the shot-line. Figure 10 shows f-x amplitude and phase spectrum of these zones. The bright strip indicates coherent signal in the phase spectrum, and the dark color on the amplitude spectrum shows coherent signal amplitude. Figures 10a) to (d) show that the frequency band is about 10-80 Hz while zone 2 is only 5-50 Hz. Figure 10e) indicates the upgoing wave (Zone 3) has a similar frequency content as the downgoing wavefield in zone 1.

The source offset of the data in zone 1 is about 410-670 m, and zone 2 is about 1200- 1880 m. The receiver depths in zone 2 are 400 to 460 m below the surface. Zone 1 is 650 to 710 m (see Figure 4). Over the most of the survey, the average shot to receiver offset is over 1400 m. The geophone depth is 700-1100 meters above the target and the frequency band is 10-70 Hz. The largely long offset data may contribute to the lower frequency bandwidths found in the 3C-3D VSP as compared with other VSP data in the area and the surface 3C-3D seismic. Casing ring was also evident on many shots. The converted wave has slightly lower signal frequency than P-wave, and more strongly contaminated with casing ring and random noise.

Time-variant spectral whitening was used to increase the frequency content of the vertical component up to 90 Hz. A nine-point filter over a scaling window of 450 ms was used.

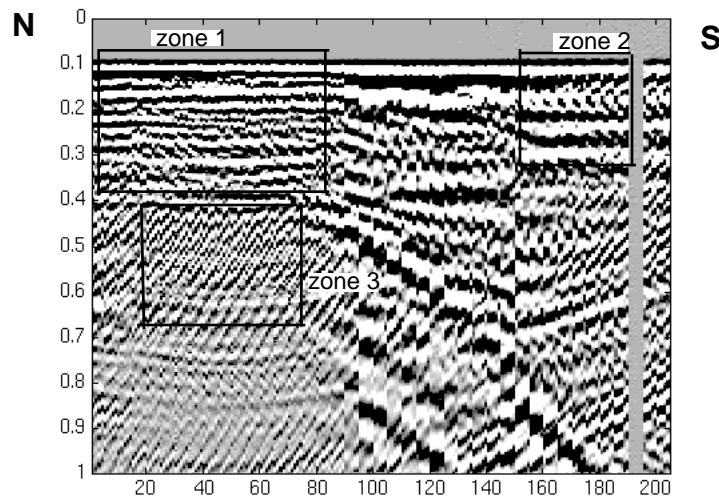


FIG. 9. Flattened vertical component data from shot - line 39.

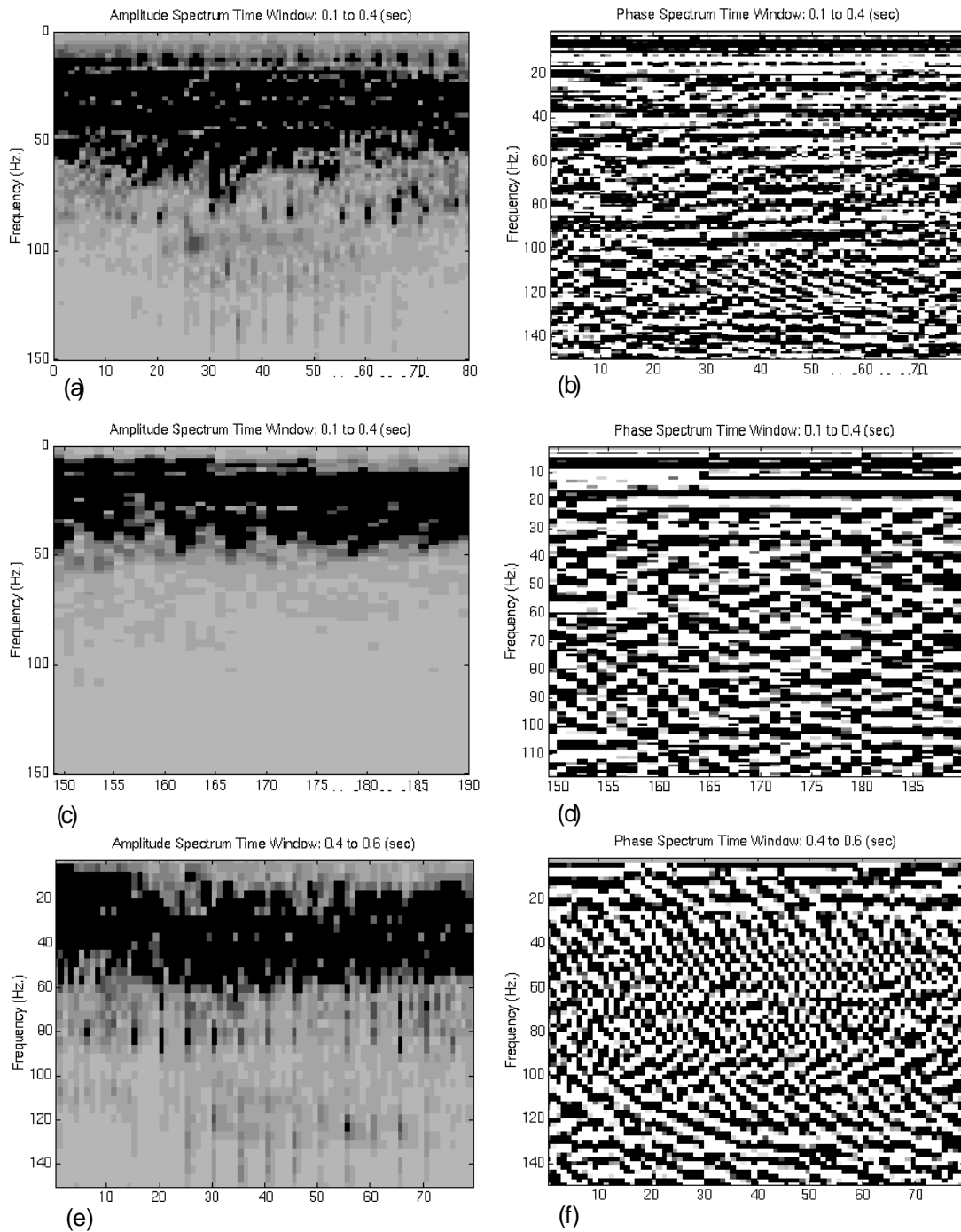


FIG. 10. Amplitude and phase spectrum of P-P wave aligned raw data from shot - line 39.

Wavefield separation and deconvolution

Wavefield separation is performed on the shot-sorted dataset. The downgoing P-wave in the vertical total wavefield is flattened using the first arrival times. A five-point median filter was applied to the entire dataset to separated the data into downgoing and

upcoming P-wave fields. This small median filter length was used to minimize shot to shot averaging of the source signature while still separating the wavefields

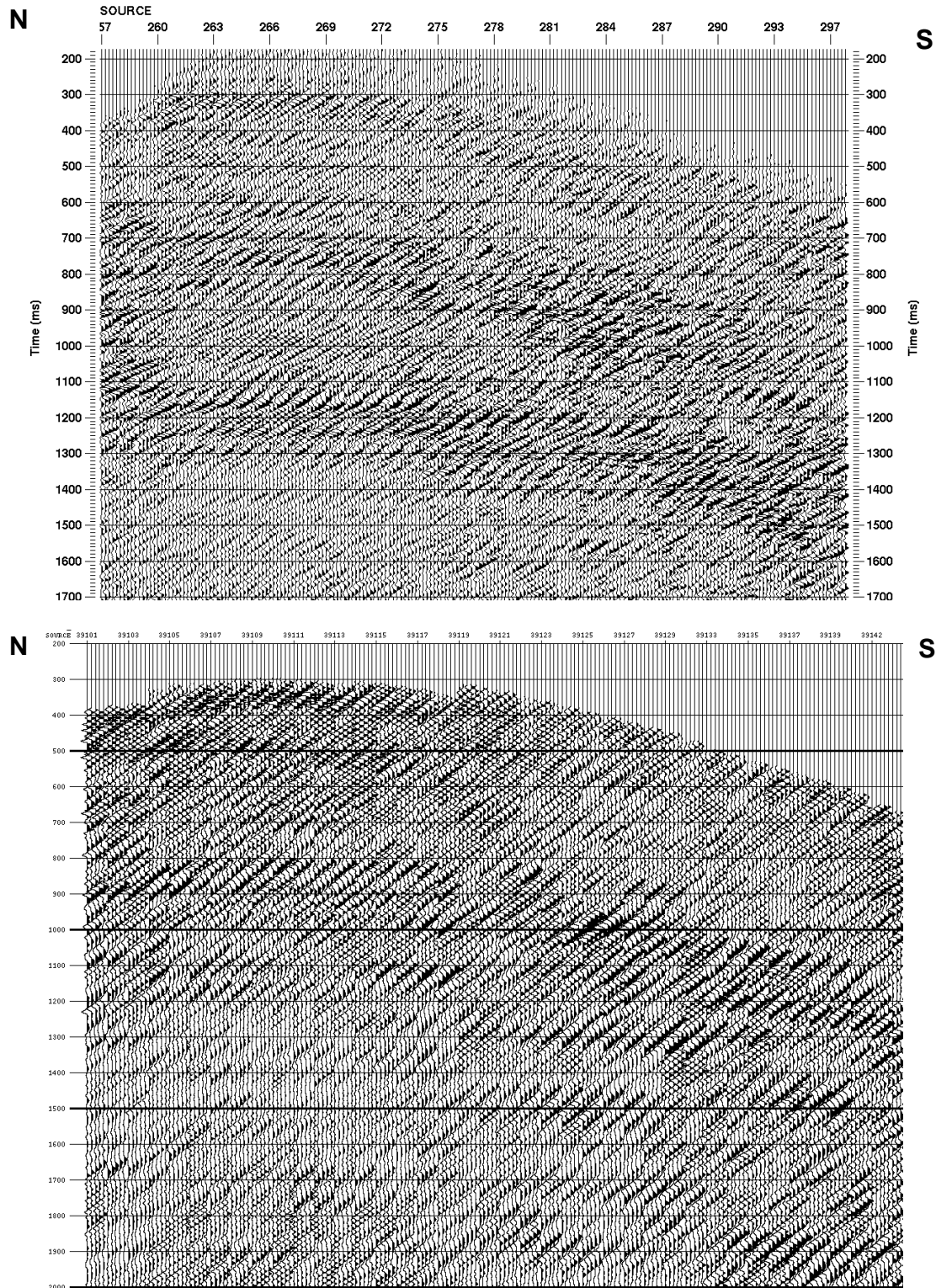


FIG. 11, 12. Vertical (top) and radial (bottom) component upgoing wave data from shot line 39. The data are screen equalized. Traces in each shot are sorted in increasing depth order.

Trace-race deconvolution operators are designed using 380 ms of the downgoing P-wave form for each depth level to shape the wave train to a bandlimited spike. These operators are applied to the corresponding reflected P-waves. This “downwave deconvolution” technique, unique to VSP data, produces a zero phase deconvolved reflection dataset which has all the multiples measured in the downgoing wavefield removed. An f-k filter then follows to reject converted upgoing waves and random noise exposed in the deconvolution process. Figure 11 shows the deconvolved upgoing P-wave reflections from shot line 39. The data are sorted in shot gathers from North to South.

The converted wave in the radial component dataset had a similar processing flow to the P-P waves. The downgoing P-P waves were separated with a five point median filter operating on the entire dataset in one pass. Downgoing converted waves were rejected with a five-point median filter. Instead of a three-point median pass on the reflected waves, a five-point was used on each shot gather to remove the strong casing ring exhibited on the horizontal channels. Figure 12 shows an example of upgoing converted-wave with deconvolution applied shot line 39. The dominant frequency is about 35 Hz.

Velocity analysis, NMO and residual statics correction

A velocity-depth model (Figure 13) is generated from the acoustic log velocities and other VSP velocity information in the area. The P-wave NMO correction is applied using the 3-DP-P wave NMO-correction method developed by Zhang et al. (1995). The fully processed upgoing P-wave and the velocity depth model are input to the NMO-correction program. The input seismic wavefield is then corrected to a two-way normal incidence P-P time in 3-D volume.

The velocity analysis is carried out by updating the NMO-corrected result. The depth-velocity model then is modified to multi-velocity functions for the total dataset. Several iterations are used in processing stage. The NMO stretch at long offsets of about 1500 m on the shallow layer (up to 0.8 s) are carefully muted.

Residual statics corrections are applied to the NMO-corrected dataset. The NMO-corrected data are sorted into common receiver domain and residual statics corrections are performed on the horizon at 1410 ms. The calculated statics are then adjusted in the shot line gather since the shots in common receiver gather are randomly located on the surface that may cause the discontinuity in receiver gather.

The velocity analysis, NMO-correction and residual statics corrections are interactively applied for several iterations to the upgoing P-wave field. Figure 14 shows the final NMO corrected result of shot line 35.

The converted-wave NMO-correction is done in the similar procedure. The P-wave velocity depth model is used here with a V_p/V_s ratio list in table 1. The upgoing converted wave fields then corrected to normal incidence P-P time. The velocity analysis and residual statics-corrections performed here are similar to P-wave. Figure 15 shows a NMO corrected shot-line 39. The discontinuity is caused by strong casing ring, which contaminated the signal. The very long offset dataset with less fold causes large NMO stretch and was partly muted on the shallow layer.

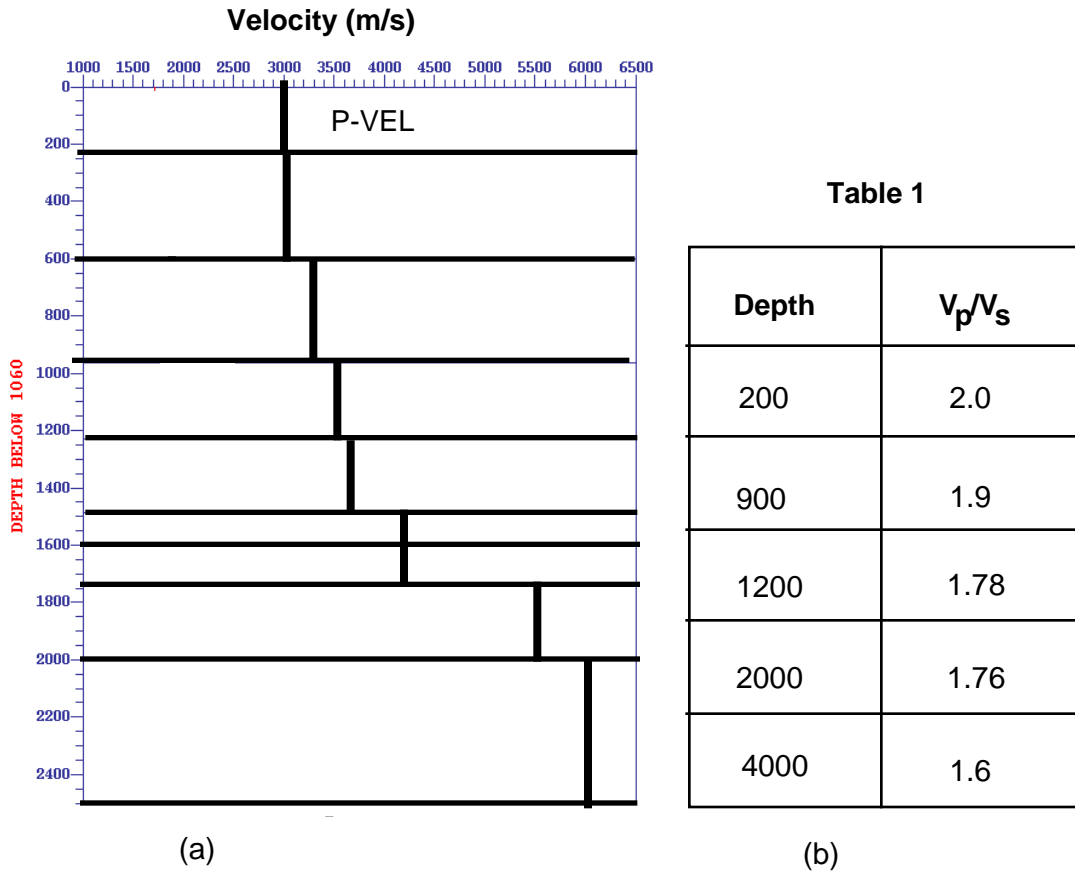


FIG. 13. (a) P-P velocity depth model. (b): V_p/V_s ration used in P-S velocity analysis

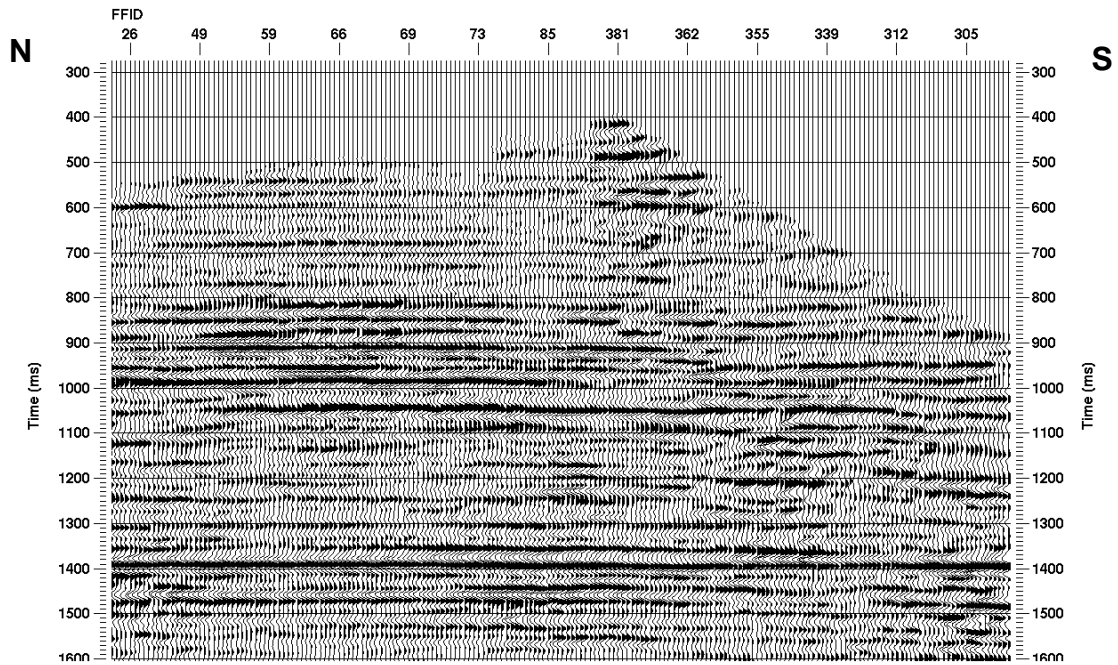


FIG. 14. NMO- and statics corrected vertical component data from shot-line 35.

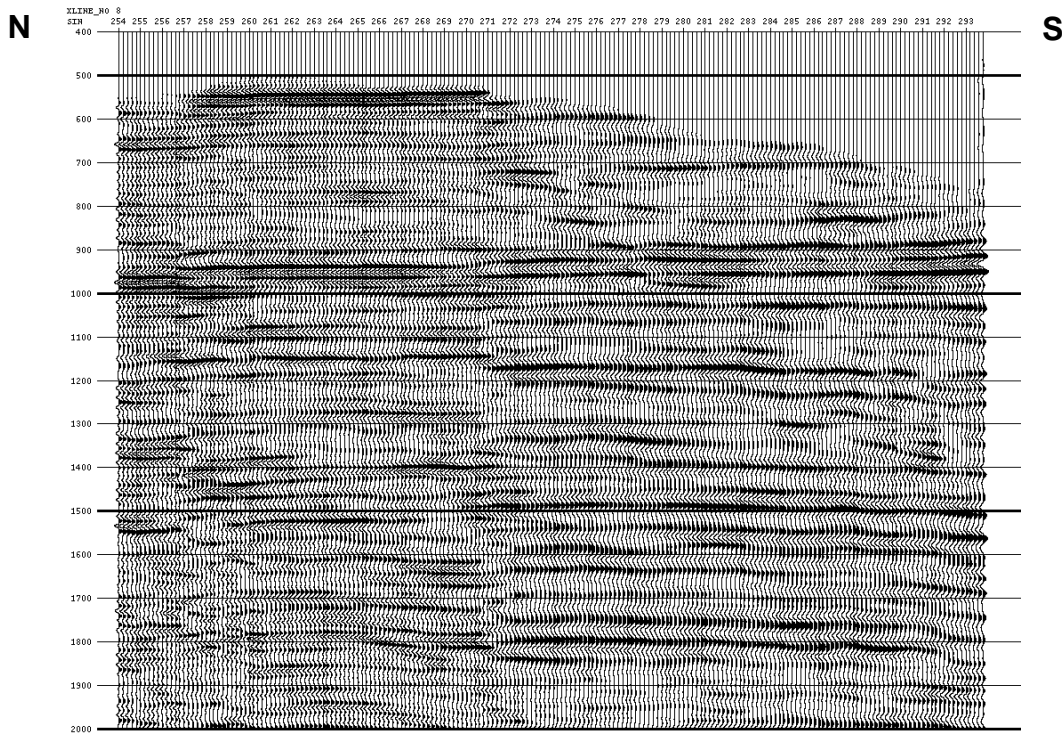


FIG. 15. NMO- and statics corrected radial component data from shot line 39.

Subsurface coverage and reflection point distribution analysis

The reflection points are offset and depth-variant in offset VSP data. The method used here to calculate the P-wave reflection points is developed by Zhang et al. (1995). This program creates a rectangular grid of bins based on a Cartesian coordinate system shown in Figure 16. The true source-receiver geometry is used to determine the subsurface reflection points. The reflection point calculated at each depth will fall in different bin cells.

Figure 17 shows the P-wave reflection point distribution at four different reflectors. The same origin, azimuths of axis are used in all displays for the comparison. The bins in these figures are 105 m by 25 m. From this figure we see the several facts. Shot geometry determines the shape of reflection coverage. Offset range of the source and receiver depth both affect the size of the reflection coverage. Fold is depend on the number of receivers as well as shots.

Figure 18 shows the converted-wave coverage at the depth shown in Figure 17. The grid is 70 by 20 m. The converted-wave subsurface coverage and reflection point distribution are the similar to the P-wave distribution but the coverage is much smaller. Table 2 shows the comparison of P-wave and converted wave coverage. Figure 18 (b) and (c) indicates the reflection point distribution on the target zone. The reflection point interval in North - South direction is 15 m with fold of 10-15 m, and 70m on the West - East direction with single fold.

From the discussion above, we learned that: the shot interval of 60 m is suitable for both P- and S-wave of 3C-3D VSP survey and gives a smaller reflection interval as compared with surface the 3C-3D surface survey. The shot line interval of 210 m is too large for 3D imaging and this interval results the large reflection intervals in West - East

direction with single fold. The number of receivers compensates for the fold in shot direction, but not in the shot line direction at target zone. The fold and the bin intervals could be improved by interpolating the shot lines with smaller intervals or increasing the number of the receivers and the receiver depth. The converted wave gives smaller coverage but closer reflection distribution, which results in higher stacking fold.

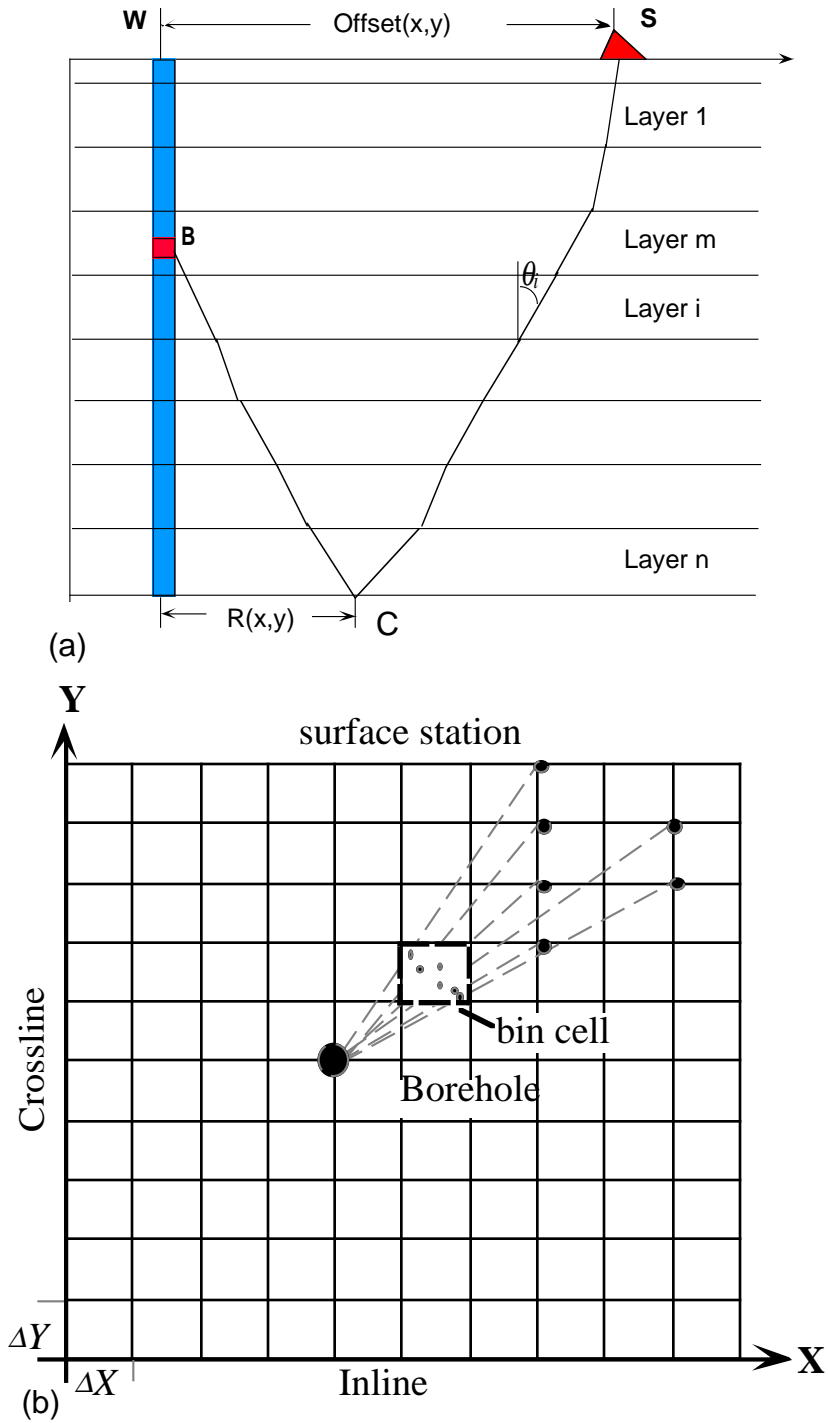


FIG. 16. The diagram showing the binning algorithm. (a): Ray geometry, (b):Surface diagram.

The Binning Method

Two depth-variant binning methods were used. The first method creates a rectangular grid of bins based on a Cartesian coordinate system. The bin origin and azimuth can be set according to surface geometry. The second method creates a grid of azimuth bins radiating out from the wellhead location. The most appropriate method for a given dataset will depend on the acquisition geometry, and the resulting pattern of reflection points. For this experiment with sparse reflection point intervals on the West-East plane, the rectangular binning method provided a better result.

The bin size of 110 by 20 m is chosen for rectangular binning. The reflection point at target zone is centered. The bin parameters chosen obey the true subsurface geometry and also give reasonable fold in shot direction and single fold in receiver line direction. The algorithm of depth variant binning (Zhang, 1995) was applied to map the reflection points and then the reflection points that fell within each bin are stacked. The converted-wave binning was done in a similar fashion. The converted wave bin size is 70 by 20 m and was centered 5 m to the left for the reflection points at target zone.

Figure 19 shows a rectangular binning and stack flowchart. The input dataset is an NMO and statics corrected dataset with stretch mute applied. Figure 20 shows four crosslines (W-E direction) CRP (common reflection point) stack sections of P-wave data. The data in each crossline are sorted in N-S direction. The x coordinates shown in this Figure are the last 4 digits of surface coordinates in W - E direction, and 5 digits in the perpendicular direction. The results shown here have F-XY decon applied and the dominant frequency of stack data is 40 Hz while the maximum frequency of the signal is 80 Hz.

The converted-wave binning and stacking are similar algorithm to the P-wave. The bin size is 70 by 20 m. The stack results are mapped to two-way P-wave travel time. (Figure 21).

Stacks and Fold distribution

For reflection imaging, the stacking fold or multiplicity is a critical parameter. The fold distribution of the P-wave at depth 1800 m is shown in Figure 22. The bin size is 110 x20 m, and the average fold is 20 while the maximum fold is about 80. Zero fold appeared on crossline number 7 due to the irregular surface shot geometry. The average fold is not as high as the surface 3D since the small number of receivers (5) in each shot gather and the large shot line interval. Overall, the fold distribution is made quite even by choosing the bin size given above.

The S-wave fold distribution is shown in Figure 23. By choosing the bin size of 70 x20 m, the average fold around target zone is about 15 while the maximum fold is about 30.

Figure 24 shows the total reflection coverage of P-wave of 3C-3D VSP. The total area shown is the CDP coverage of P-wave of surface seismic image. The well plotted on the map is based on bottom hole location. The VSP data was acquired in the undeviated portion of the 12-16 well which is close to the 09-17 well on the surface location. From this map we see 3D VSP gives a limited areal coverage depending on the shot location on the surface. The maximum coverage is less than a quarter of the surface seismic coverage.

RESULTS

The objectives of the Blackfoot 3C-3D survey were to determine if clean channel sands (incised valley fill sediments within the Glauconite Formation of Lower Cretaceous, Miller et al., 1995) could be distinguished from shale-plugged channels and regional non-channel sediments.

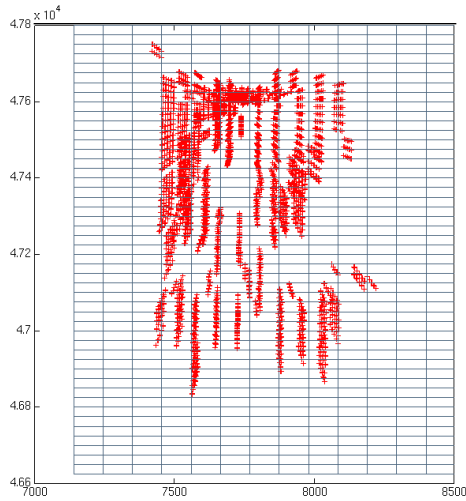
This interim report describes only P-P wave correlation of the VSP data with surface 3D data. Figure 25 shows the integrated display of different seismic data at Blackfoot. A synthetic seismogram generated from well Log 9-17-23-23W4 with normal polarity is plotted on the left and annotated with formation tops. A part of crossline 9 of 3D VSP P-P wave stacked section is shown in the middle panel. Data is displayed in the North-South direction. A part of the surface 3D seismic inline section 51 located in the identical location is shown in the right panel, and the traces in this section are sorted from South-North direction. The plot shows that 3D-VSP has a similar frequency content as compared to the surface 3D seismic, and they tie to each other very well at all formation tops. The seismic characteristics of the Glauconite formation (above the Mississippian) on 3D-VSP section (middle) is quite similar to that on the surface 3D seismic data. The character change over the Glauconite formation zone indicates the possibility of changing from non-channel sediments to clear channel sands.

CONCLUSION

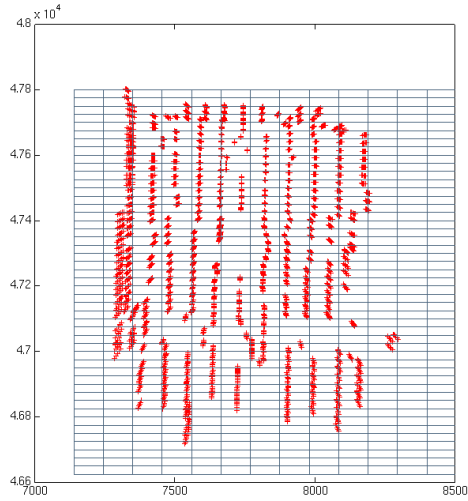
The Blackfoot 3C-3D VSP indicates that 3-D VSP is a practical seismic tool. When combined with surface seismic acquisition, it is also an efficient and cost-effective method of obtaining additional seismic information in the time-depth domain. We have developed processing procedures which include signal analysis, wavefield separation, statics correction, moveout correction, depth-variant binning and stake. A good correlation of the 3-D VSP with the surface seismic images and well log synthetics was generated. The frequency content is diminished by the primarily long offset geometry of this study. Better results would likely be obtained through improving the source receiver geometry by either increasing the surface shot line density or increasing the receiver depth coverage in order to produce a smaller bin size. The objectives of both the surface and borehole surveys must be kept in mind when designing the acquisition parameters in order to achieve the best results.

REFERENCES

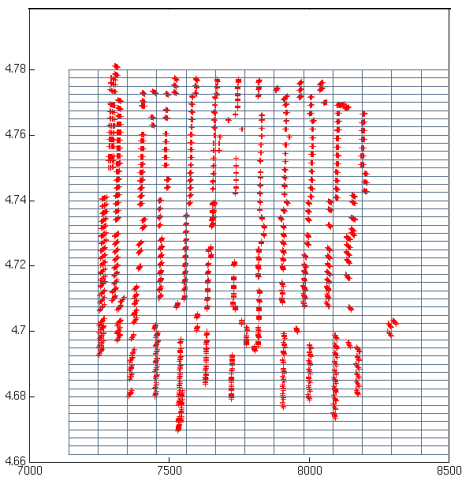
- Gorek S., Stewart, R. R., and Harrison, M. P., 1995, Processing the Black foot broad-band 3-C seismic data: CREWES Project Research Report, V. 7 Chpt. 38.
- Margrave, F. M., 1995, Estimates of the signal band of the Blackfoot broad-band data: CREWES Project Research Report, V. 7 Chpt. 39
- Miller, S. L. M., Aydemir, E. O. and Margrave G. F., 1995, Preliminary interpretation of P-P and P-S seismic data from the Blackfoot broad-band survey: CREWES Project Research Report, V.7, Chpt. 42.
- Zhang, Q., Stewart, R. R., and Sun, Z., 1995, 3-D VSP: Survey design and processing: CREWES Project Research Report, V.7, Chpt. 34.



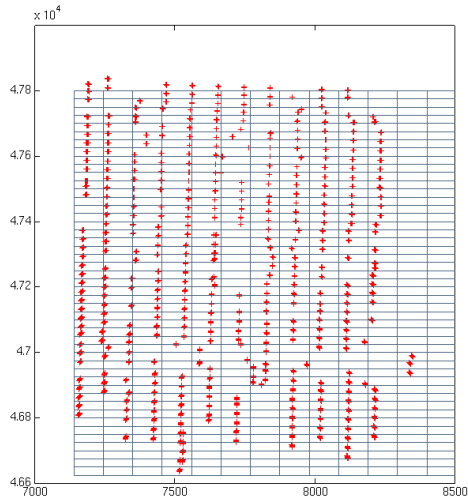
(a): Depth 955m, time 600 ms



(b): Depth 1530 m, time 900 ms

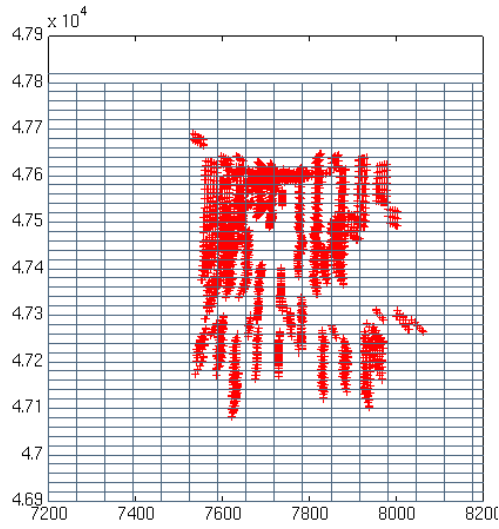


(c): Depth 1764 m, time 1018 ms

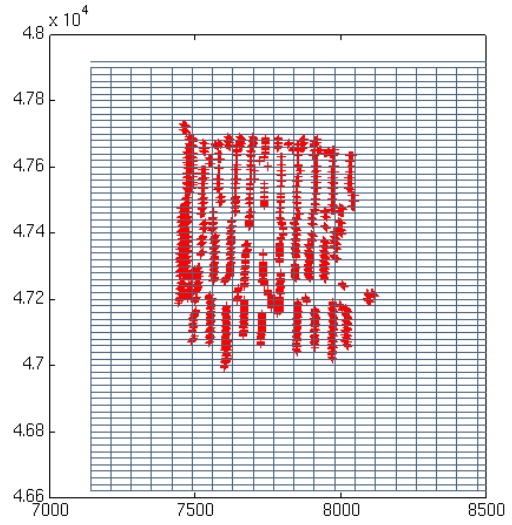


(d): Depth 2988m, time at 1452 ms

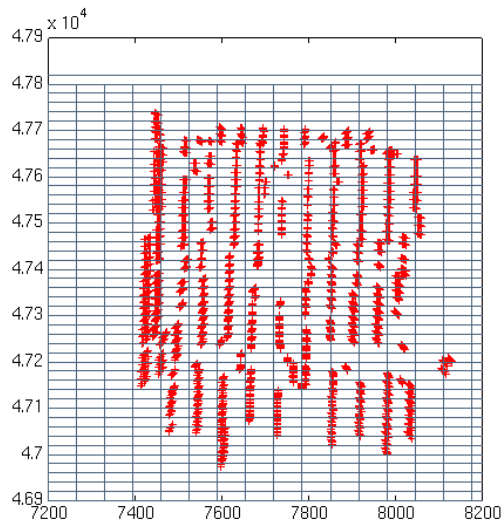
FIG. 17. P-wave reflection point distribution for different depths.



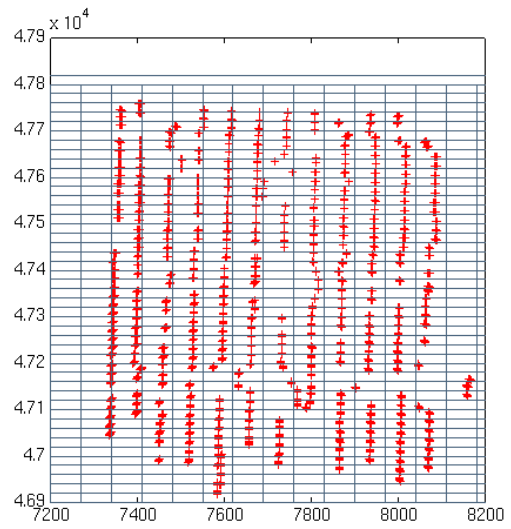
(a): Depth 955 m, time 600 ms



(b): Depth 1530 m, time 900 ms



(a): Depth 1750m, time 1200 ms



(a): Depth 2988 m, time 1440 ms

FIG. 18. SV-wave reflection point distribution for different depth.

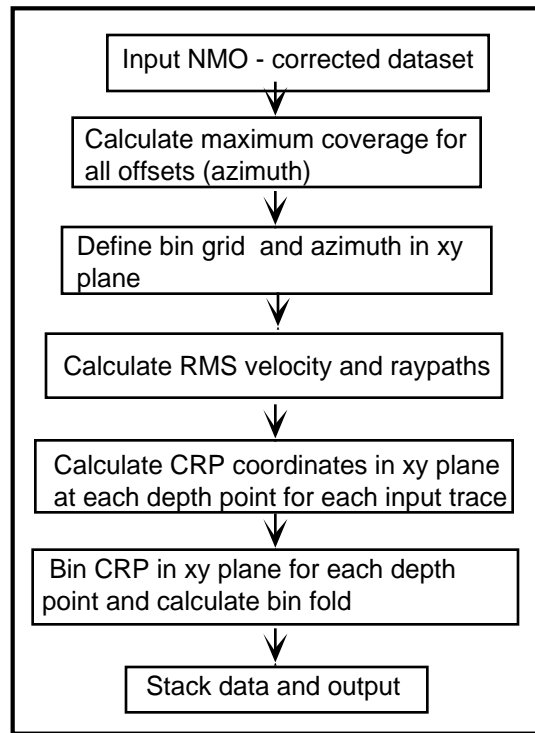


FIG. 19 3-D VSP P-P wave binning and stacking flowchart.

Layer depth (m)	P-P wave coverage (x,y) (mxm)	% of surface coverage (%)	P-SV wave coverage (x,y)(mxm)	% of surface coverage (%)
955	650 x 830	8.3	480 x 560	4.15
1530	900 x 1000	13.8	600 x 700	6.46
1760	1000 x 1100	16.9	640 x 720	7.08
3000	1170 x 1200	21.5	720 x 860	9.54

Table 2. The subsurface coverage of P-P and P-S wave of 3C-3D VSP

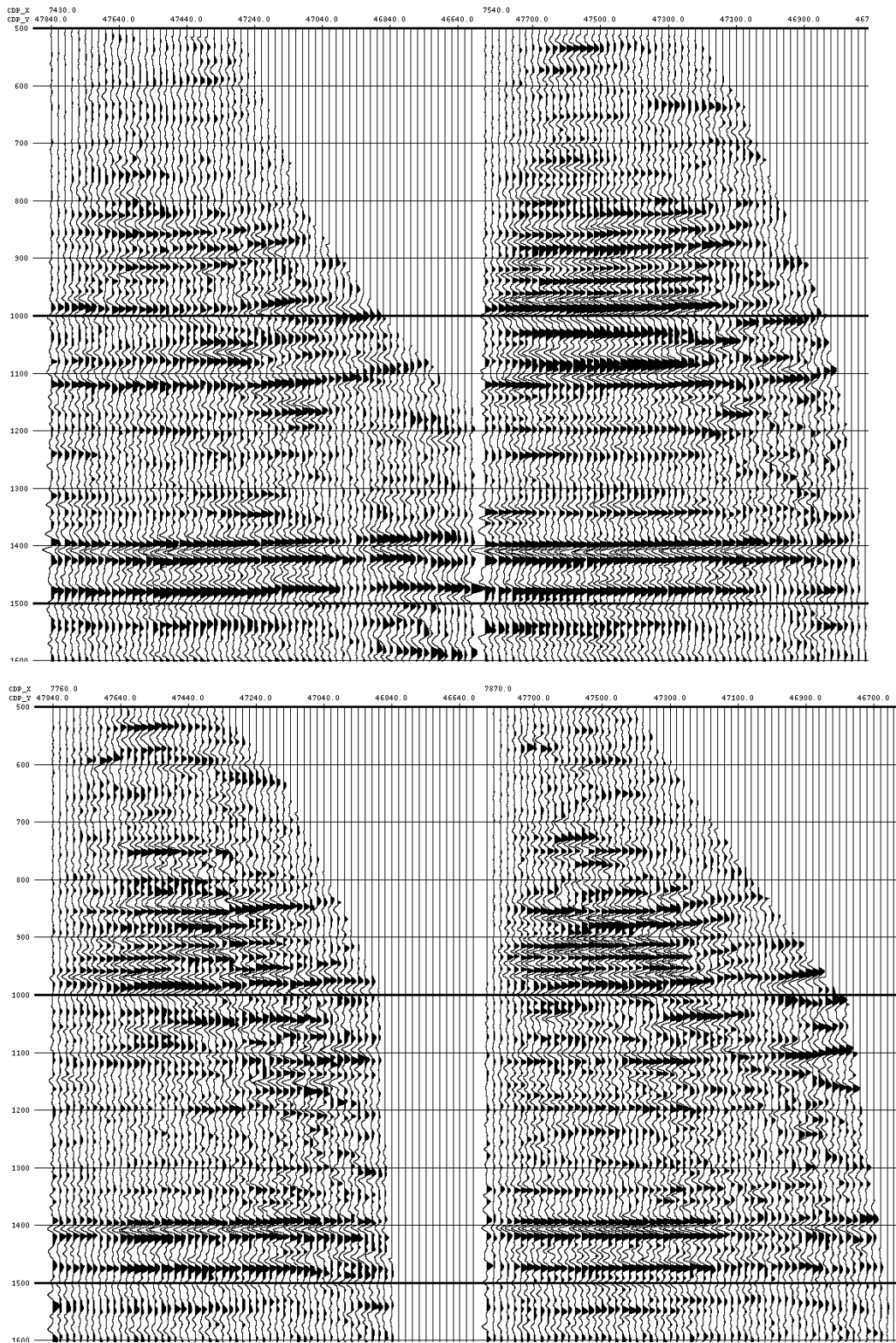


FIG. 20. Stack crossline (W-E) sections of vertical component data. Traces in each line are sorted in N-S direction. Bin size(x,y): 110 x 20 m.

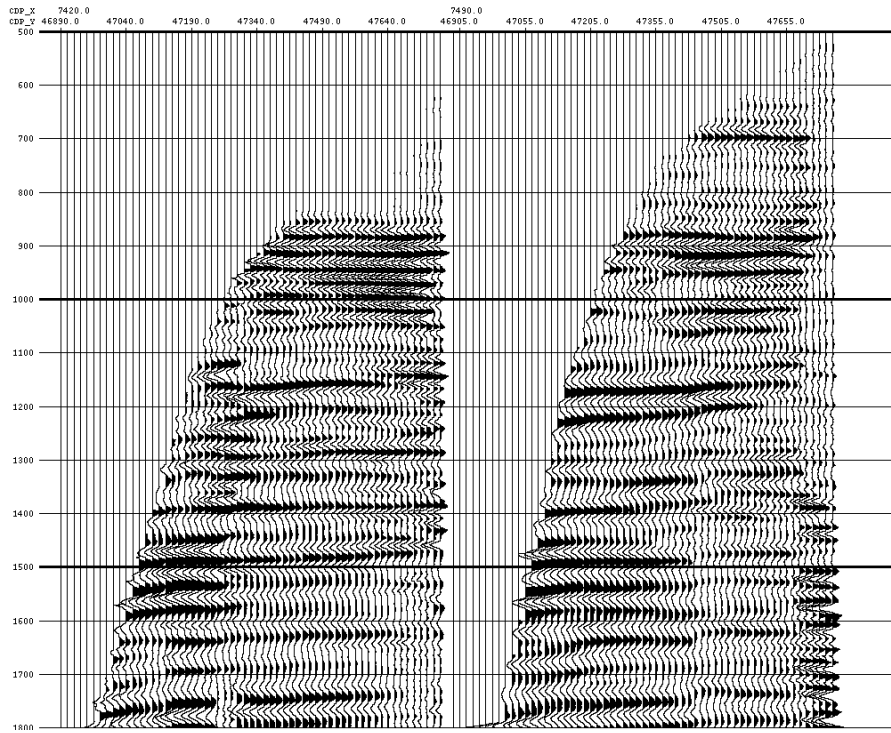


FIG. 21. Crossline stack section of radial component. Data in each line are sorted in S-N direction.

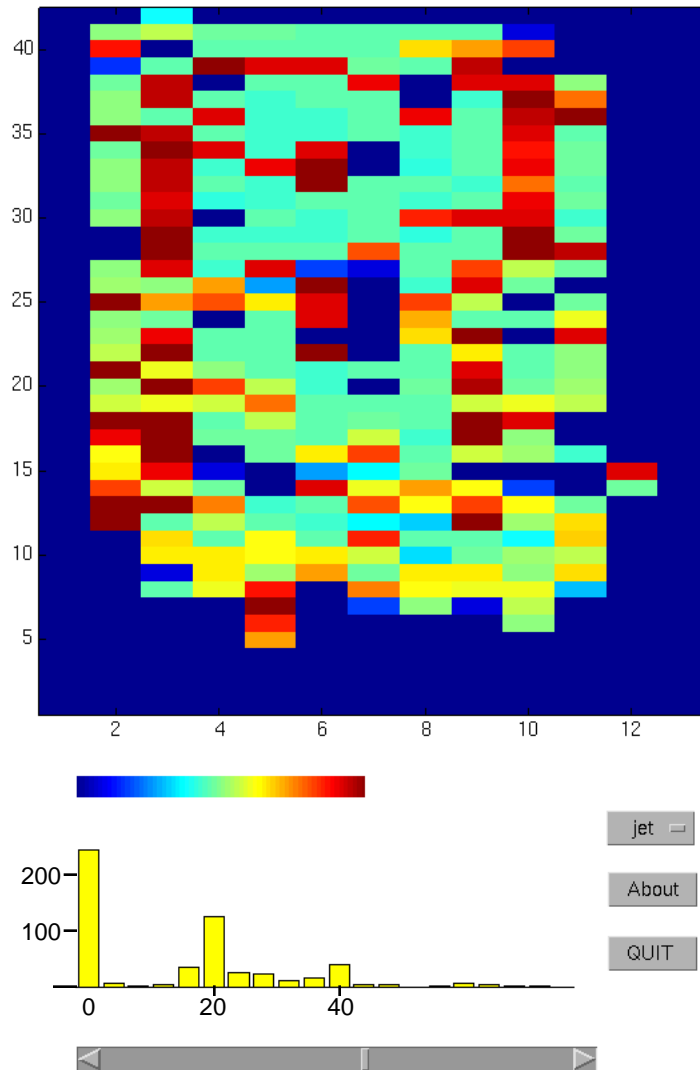


FIG. 22. Fold distribution of vertical component. Bin size is 110 x 20 m Depth 1800 m time 1018 ms

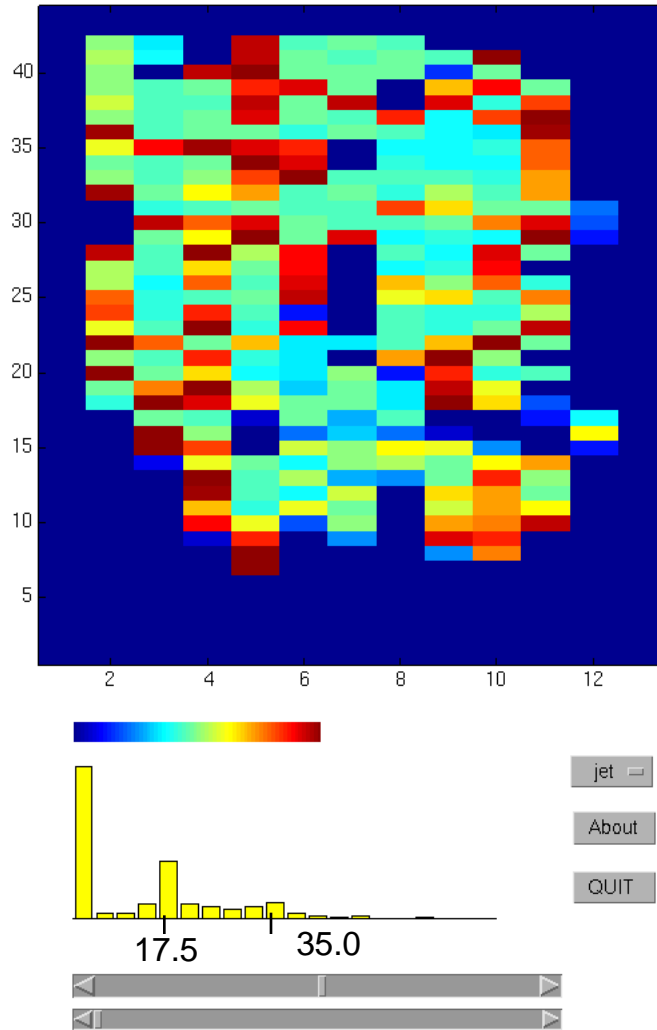


FIG. 23. Fold distribution of radial component. Bin size is 70 x 20 m, at depth of 1200 m.

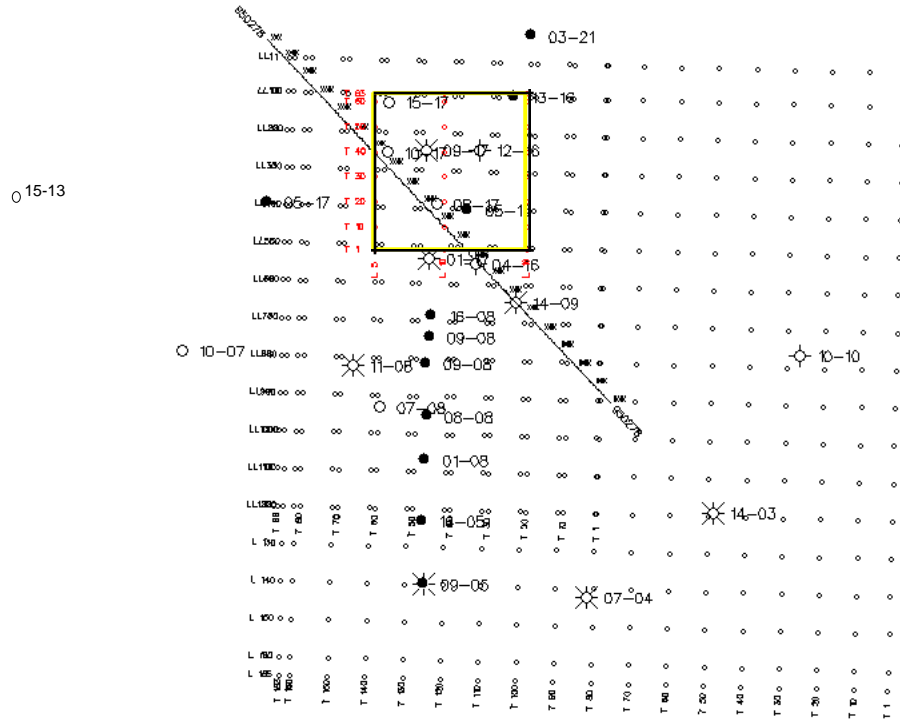


FIG. 24. The subsurface coverage of P-P wave of 3C-3D VSP, Blackfoot

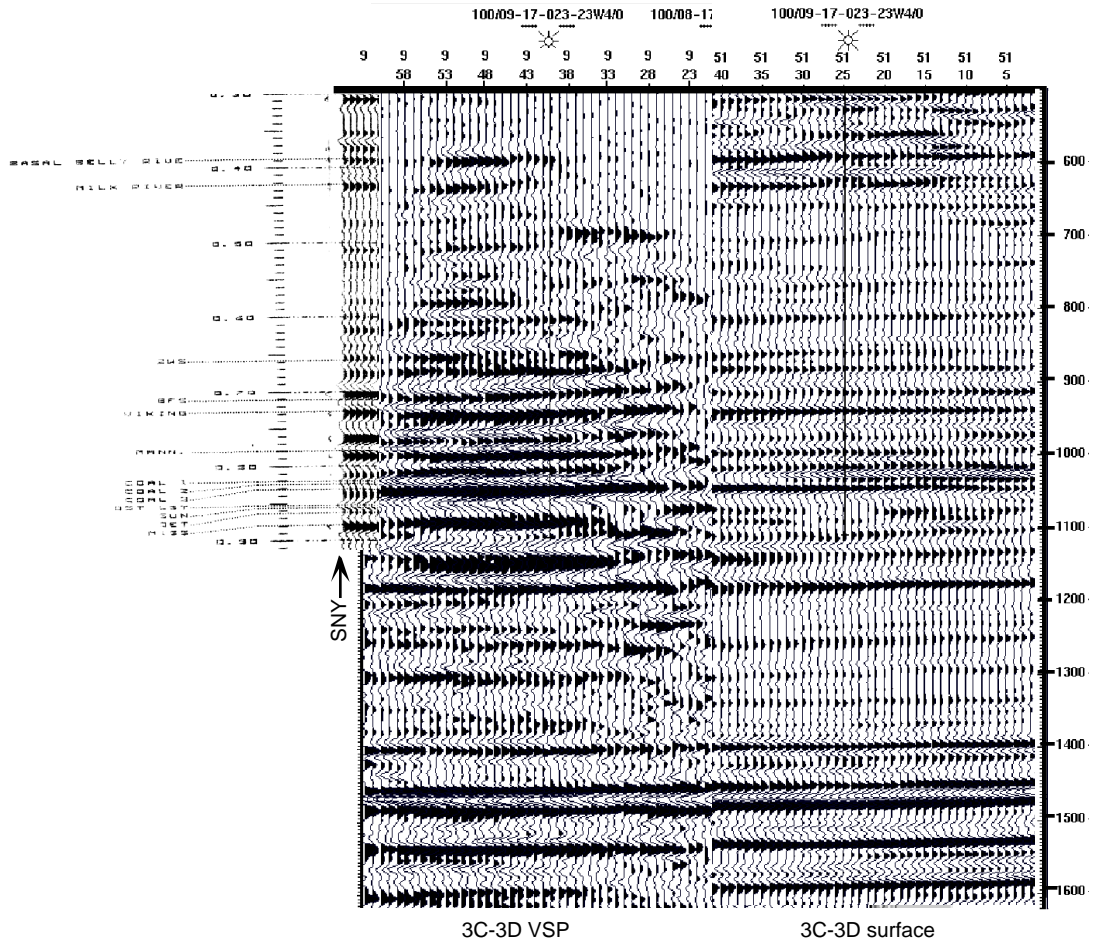


FIG. 25. The integrated display of P-Wave seismic data and synthetic from well Log 9-17-23-23W4. The VSP and surface data are mirror images.